

SIGNATURES OF INTERNALLY GENERATED LANDER VIBRATIONS

One of the disadvantages of placing the Viking seismometer on the Lander was that large amounts of noise were expected from mechanical vibrations of Lander machinery and electrical cross talk. It was important to identify these noise sources so that they would not be confused with externally generated events.

The following figures A-5 through A-11 show examples of internal noise sources that have been identified. In addition, figures A-12, A-13, and A-14 show examples of noise generated within the seismic package itself.

APPENDIX FIGURE CAPTIONS

- FIGURE A-1. Crustal thickness map of Mars from orbital gravity data. This map (from Phillips and Tiernan, 1977) assumes an average crustal thickness of 100 km and a density contrast of 0.3 gm/cm^3 .
- FIGURE A-2. Change in calibration pulse amplitude versus time. Decrease of temperature within the lander is believed to have caused an increase in sensitivity of the calibration and transducer coils by decreasing their resistance. All components still are matched within 5%.
- FIGURE A-3. Schematic top view of the lander showing the location of the seismometer and the axis of rotation inferred from the coherence of signals observed by the seismometer.
- FIGURE A-4. Schematic side view of the lander in a plane perpendicular to the axis of rotation. Seismic motion implies that the lander tends to rotate around an axis through footpads 1 and 2.
- FIGURE A-5. Soil Sampler motions. The sample arm is the noisiest device on the lander. The example of sampler activity shown (in Event mode) covers a period when the arm is extended, stopped, and retracted. The nearly exponential amplitude decay near the middle of the record occurred when the sample arm was stopped near full extension. As the arm was brought back towards the

*Need explanation of each of ^{data} 6 traces & 2 time traces.
for Figs A-5-*

lander the increase in resonant frequency is reflected in the increase in zero crossings. When extended, the arm resonates at a frequency of from 2 - 4 Hz, depending on the extension, and with a Q of about 250. When the arm is not being used it is retracted and does not vibrate. Since the arm is only used for short periods of time, its vibrations do not seriously affect the acquisition of seismic data. The collector head vibrator on the sample arm operates at 8.8 and 4.4 Hz. Both of these signals are clearly visible on seismic records when the vibrator operates.

FIGURE A-6. S-Band antenna motions. The S-Band antenna is a large dish antenna on a 2 meter pole attached to the lander about 10 cm from the seismometer. When in use, the antenna is rotated to track the Earth. The sample shown in the figure is Event mode data showing the initial slew of the antenna from its parked position to its Earth-pointing position followed by periodic steps of the drive motor while following Earth (every 30 sec). The frequency observed by the seismometer is 7.6 Hz with a Q of about 25. Since the antenna is seldom in use, its effect on seismic data is negligible. However, it is probable that Martian winds are coupled to the lander through the antenna.

FIGURE A-7. S-Band antenna operation recorded in normal mode. Note that the amplitudes recorded are much lower than in Event mode.

This is due to the difference in response of these two modes; the Event mode being more sensitive to high frequencies.

FIGURE A-8. Camera motion. The Viking cameras make vertical scans of the area to be photographed and rotate slowly to complete a scene. The seismometer in Event mode records this operation as a low-level amplitude and a frequency of 7.1 Hz. Since the lander tape recorder is running continuously while the camera is operating, the noise seen by the seismometer could be caused by the tape recorder.

FIGURE A-9. X-ray Experiment Sample dump. When the X-ray Fluorescence Experiment clears its sample chamber, the vibrations of the trap door are visible as low level signals on the amplitude traces and about 5 Hz signals on the axis crossing traces.

FIGURE A-10. Tape recorder motion. When the Lander Data Storage Memory (DSM) buffer is full, it is dumped to the lander tape recorder. This operation is observed by the seismometer as bursts of noise at 7.3 Hz lasting for about 15 sec.

FIGURE A-11. Cross talk with Meteorology Experiment. Each time a sample is obtained by the Meteorology Experiment, an electrical pulse is registered by the seismometer usually causing a one bit signal on each axis in the Event mode. In the sample shown,

Meteorology is taking samples every 8 seconds. The noise produced is most easily seen on the Y component axis crossing trace. Because of the low level of this interference, it is not considered serious.

FIGURE A-12. Electrical transient noise produced in the seismometer package. The noise observed correlates well with the time of the beginning of each record. It is most serious in High Data Rate when a record lasts only 4 seconds. Because this noise is exactly reproducible, it could easily be removed from the data.

FIGURE A-13. Gain change transient, 0-30 db. When the seismometer gain is changed, an electrical pulse from the amplifier is passed through the system. This pulse is an instrument characteristic and is easily recognized.

FIGURE A-14. Gain change transient from 36 db to 0 db. Case must be taken when the instrument is in normal mode when the triggers are enabled because this transient will cause the system to trigger into the Event mode.

FIGURE A-15. 'I' event in High Data Rate. 'I' (or Impulsive) events are believed to be generated by sharp motions of the lander, possibly related to relief of thermal stress.

FIGURE A-16. 'I' event in the High Data Rate. This event differs from

A-15 & A-16 are electrical cross-talk from meteorology external (sensor heater switches)

the previous one in that motion is almost completely confined to the Y-direction, while in the above event motion was in the X-Y plane. This observation shows that 'I' events can originate in different parts of the lander.

FIGURE A-17. 'I' events recorded in the Event mode. These events show similar properties from one event to the next, indicating that they all came from the same source. Although their source is most likely in the lander, it is not yet identified.

FIGURE A-18. Correlation of wind speed with seismic noise on Sol 10. Wind gusts of 8 - 9 m/sec produced seismic amplitudes of 8 - 10 DU. Detailed correlations are difficult because the seismic amplitudes are 1 second averages and the wind speeds are widely spaced point samples.

FIGURE A-19. Correlation of wind speed with smoothed amplitude of Event mode seismic data. The solid line shows the expected slope if the seismic amplitude is proportional to the square of the wind speed. The high degree of correlation is in agreement with this relationship.

FIGURE A-20. Correlation of wind speed with high data rate seismic amplitude. In the high data rate, where no averaging is involved, seismic noise also correlates with the square of the wind speed.

FIGURE A-21. Axis Crossing histogram for Sol 133 event. The number of events is related to the amount of signal at that frequency. Because the shape of the histogram reflects the response of the system it can be assumed that the wind noise produces a nearly flat spectrum and lander resonances are not important.

FIGURE A-22. Axis Crossing histogram for Sol 139 event. This event is similar to the 133 event but slightly richer in high frequencies.

FIGURE A-23. Spectral estimates of Event mode amplitude for Sol 131 during a 51-minute period starting at 20:15:34. The slow decrease in power with increase in frequency is typical of wind noise. The numbers to the right of the figure are the actual spectral estimates with the 32 values for the X axis in the top two rows.

FIGURE A-24. Sol 12, 16:50 LLT event. This event, and those in the 5 following figures, were chosen as possible marsquakes when first observed (also Figures 21 and 22 in text). Chosen mainly for their impulsive beginnings, these events were believed to have characteristics expected for marsquakes. However, all but two have been correlated with wind gusts. This event occurred at a time when no wind data was available. The high background level and its occurrence at a time of day when wind gusts are common make it highly probable, however, that this is a wind generated event. Additional information on these events is found in Table 3 in the text.

FIGURE A-25. Sol 23 15:15 LLT event. This event correlates with a 12 m/sec wind gust.

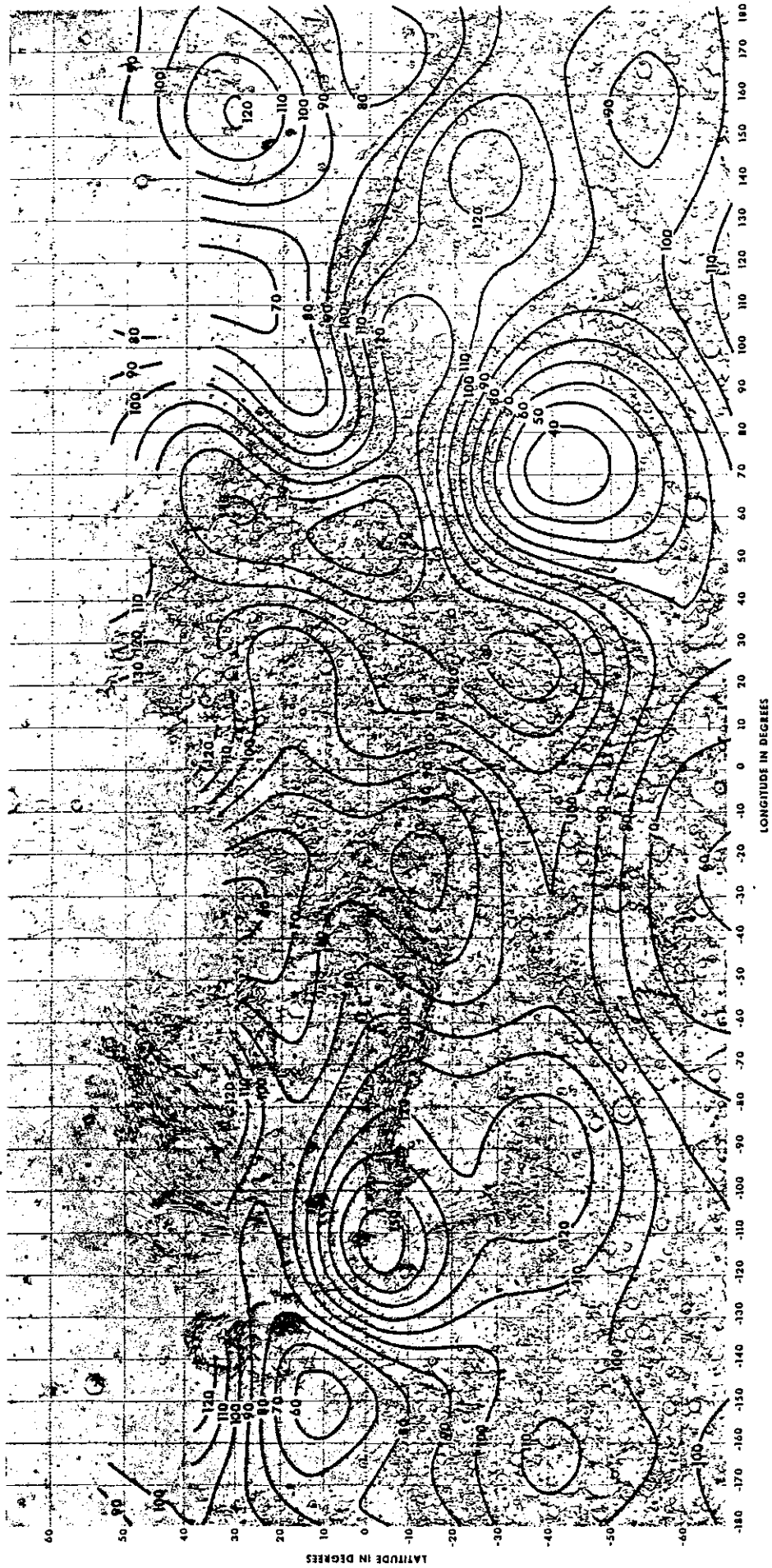
FIGURE A-26. Sol 42 15:54 LLT event. This event correlates with a 11 m/sec wind gust.

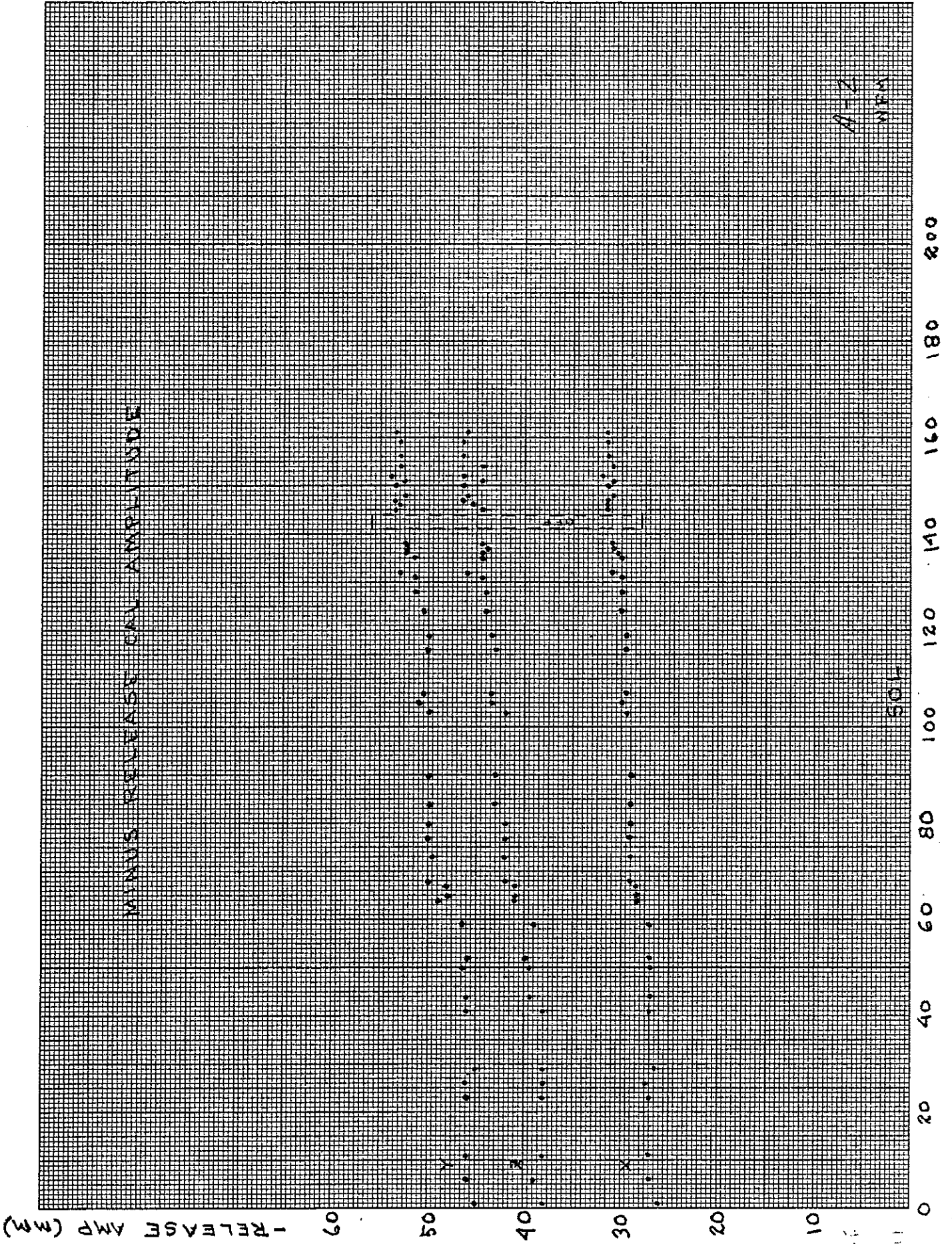
FIGURE A-27. Sol 49 13:45 LLT event. This event correlates with a 12 m/sec wind gust.

FIGURE A-28. Sol 49 14:35 LLT event. This event correlates with an 8 m/sec wind gust.

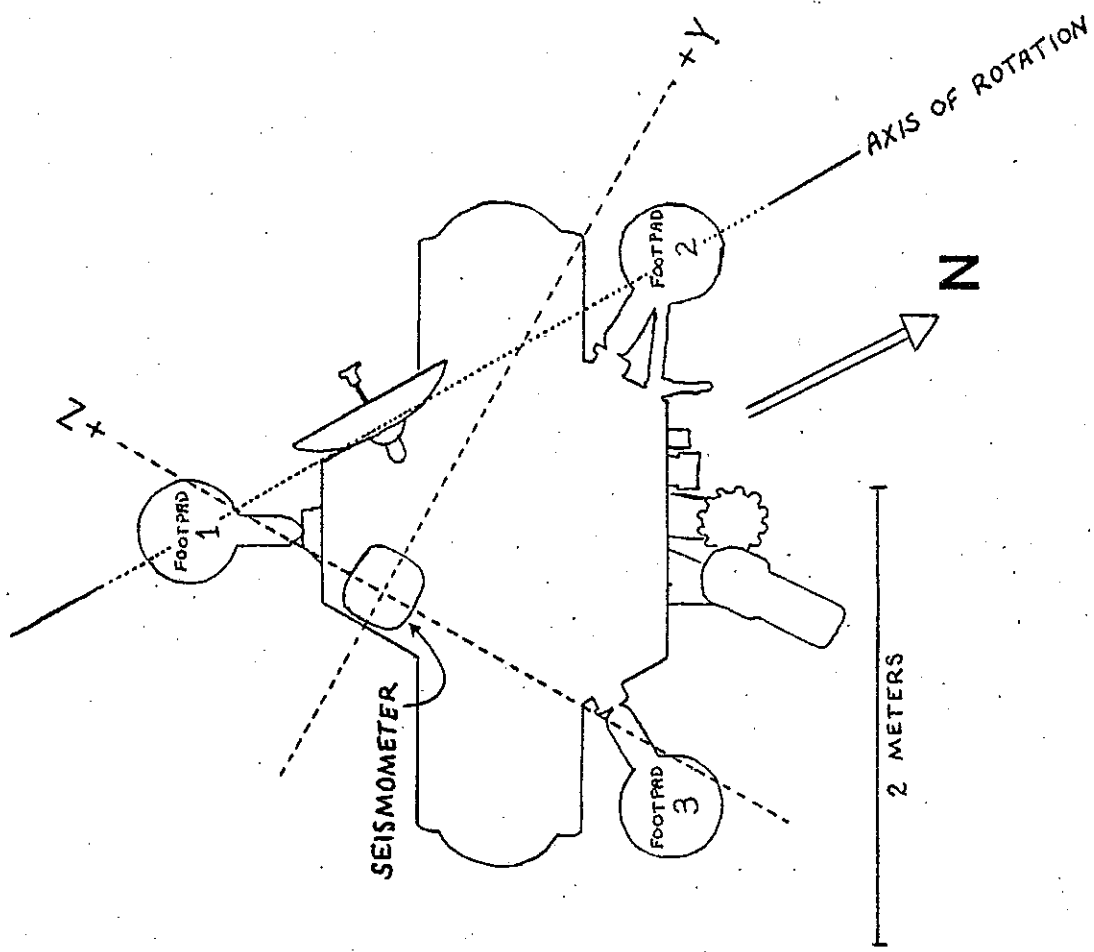
FIGURE A-29. Sol 49 15:48 LLT event. This event correlates with a 10 m/sec wind gust.

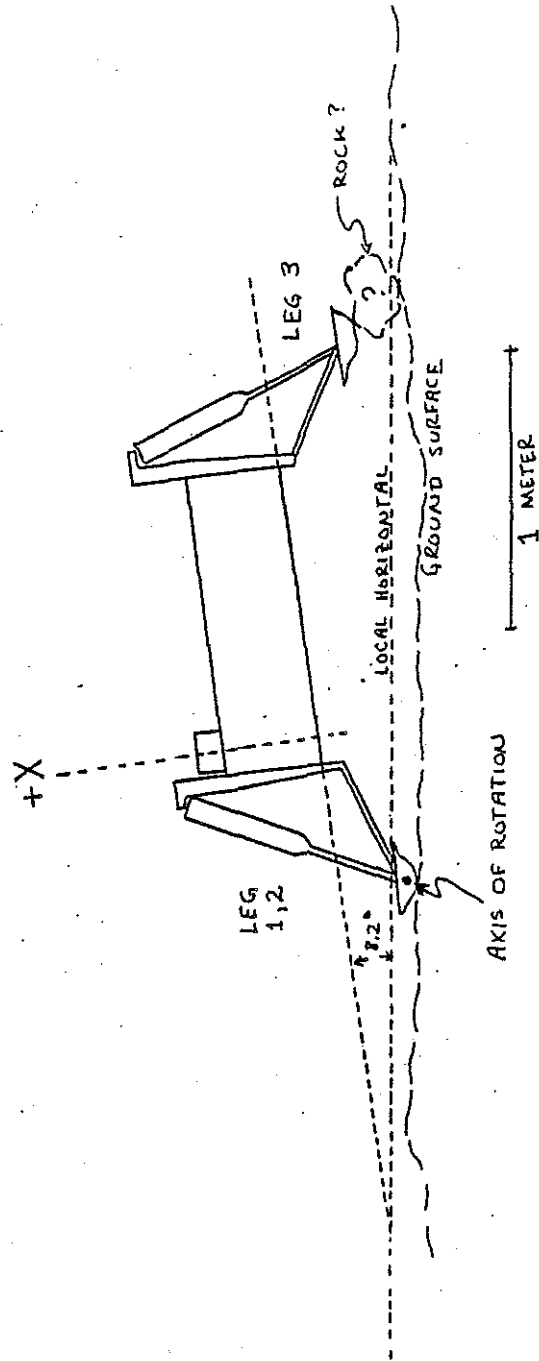
ISOPACH MAP WITH MEAN CRUSTAL THICKNESS OF 100 KM.

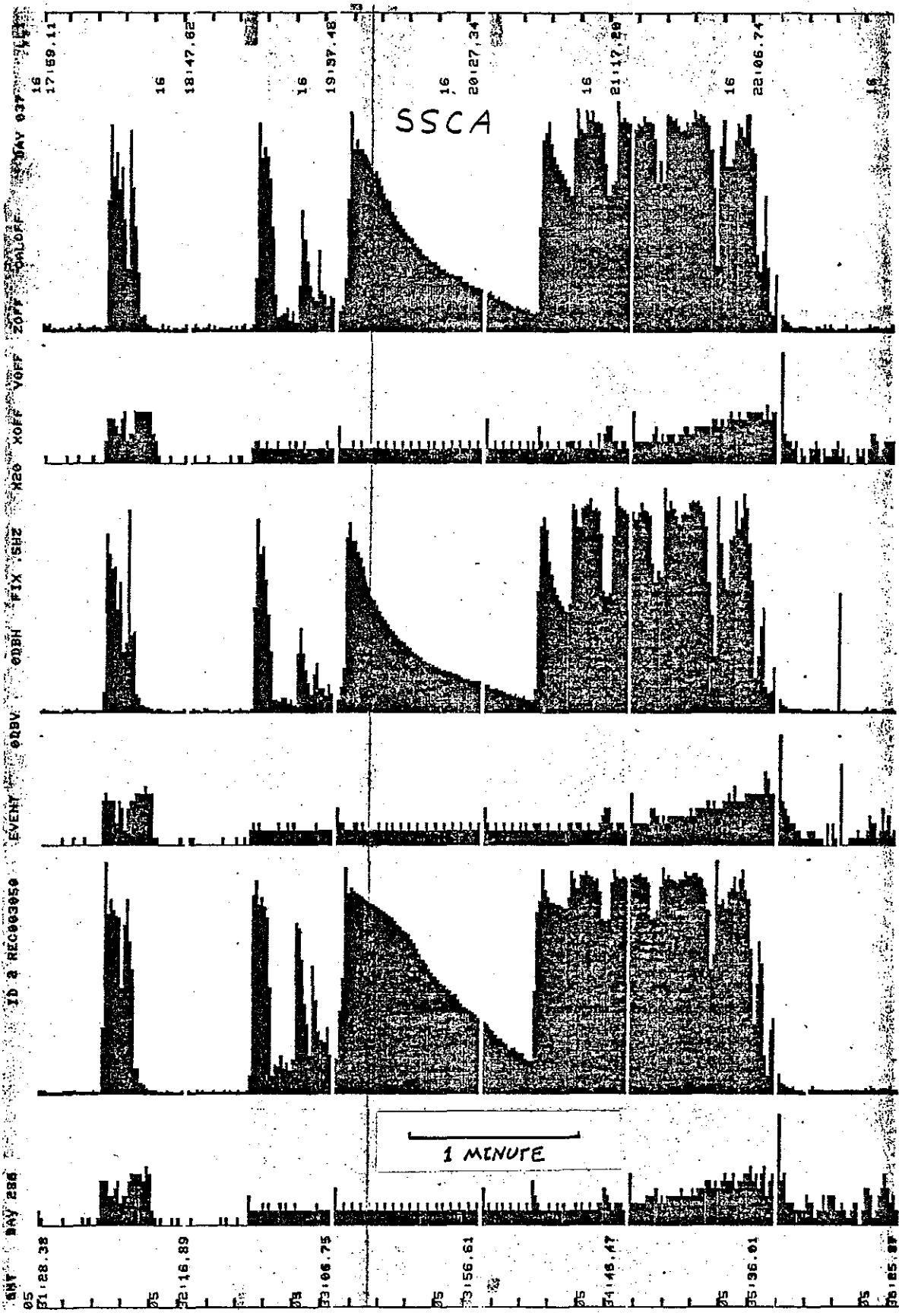




A-2
MFM

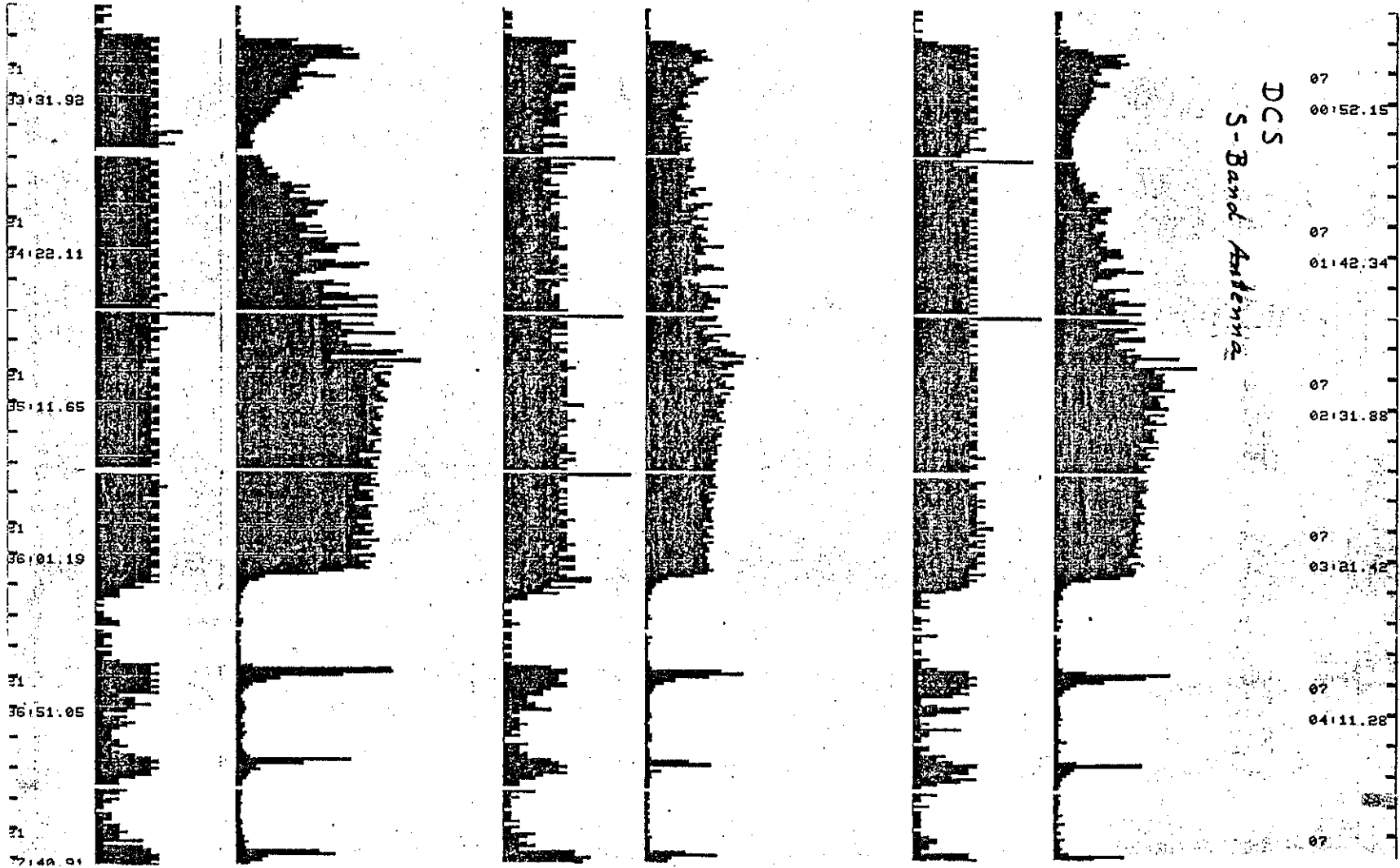




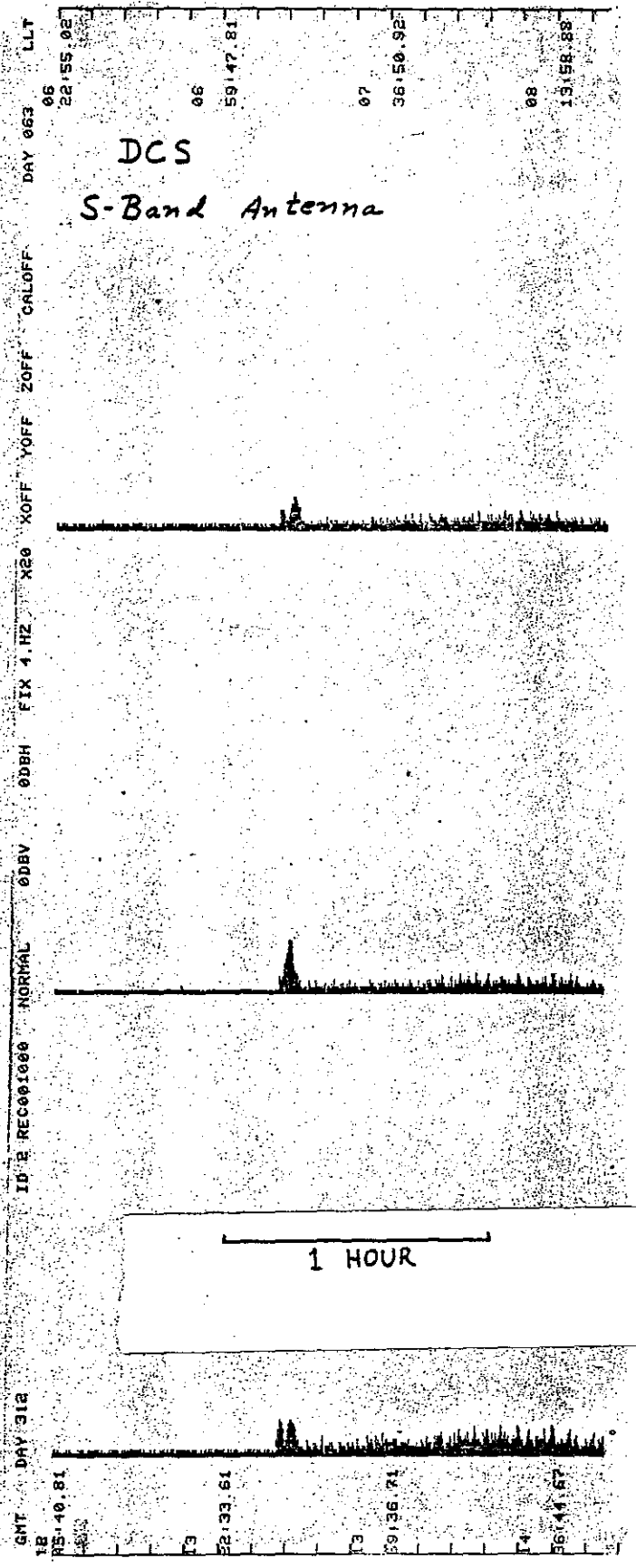


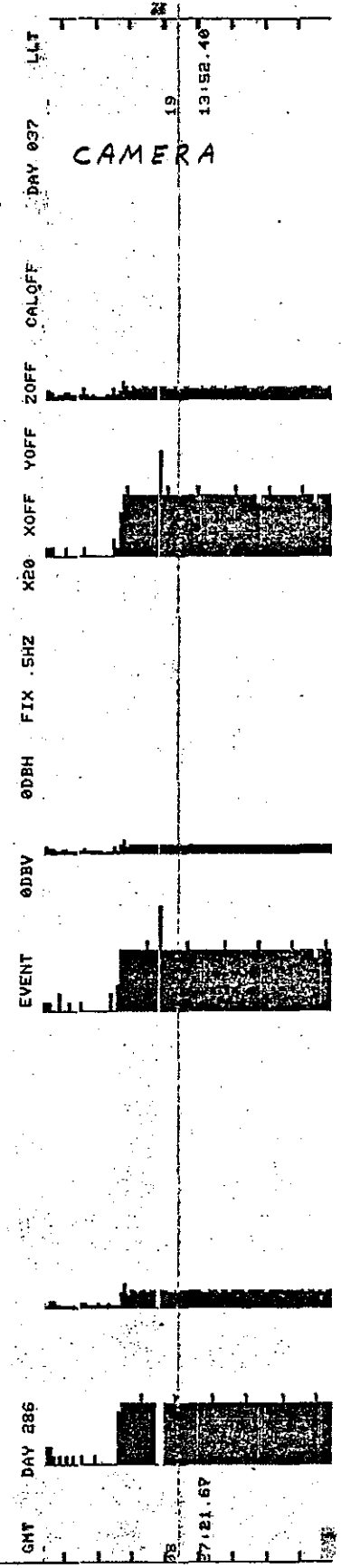
GMT DAY 286

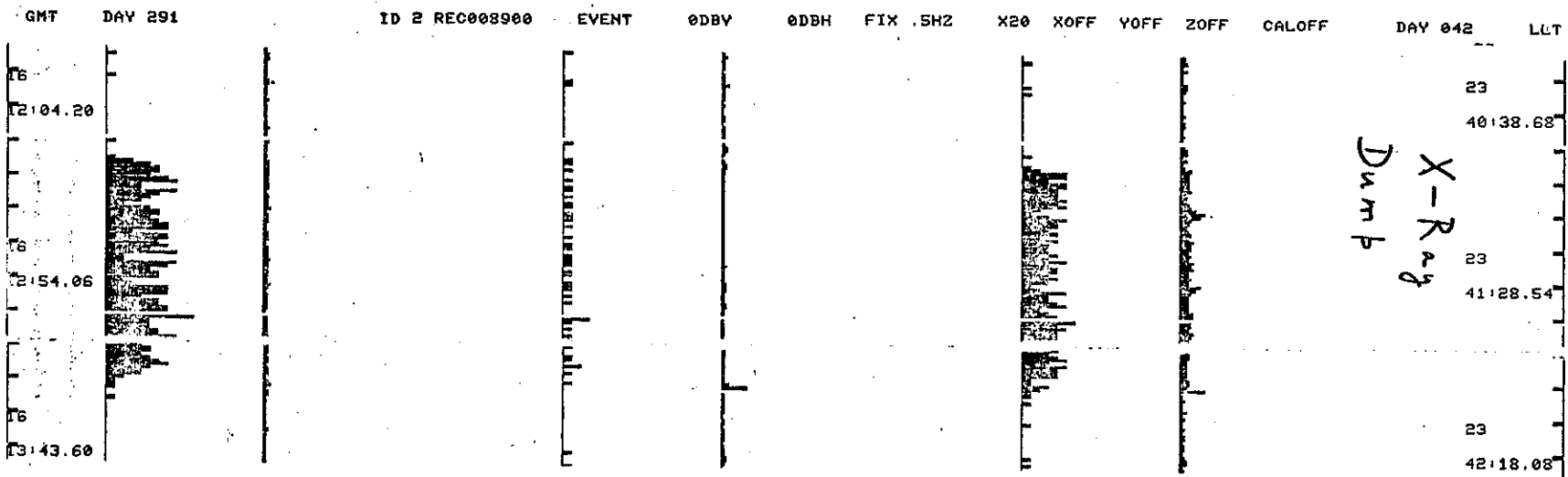
EVENT 0DBV 0DBH FIX .5HZ X20 XOFF YOFF ZOFF CALOFF DAY 038 LLT



A-6



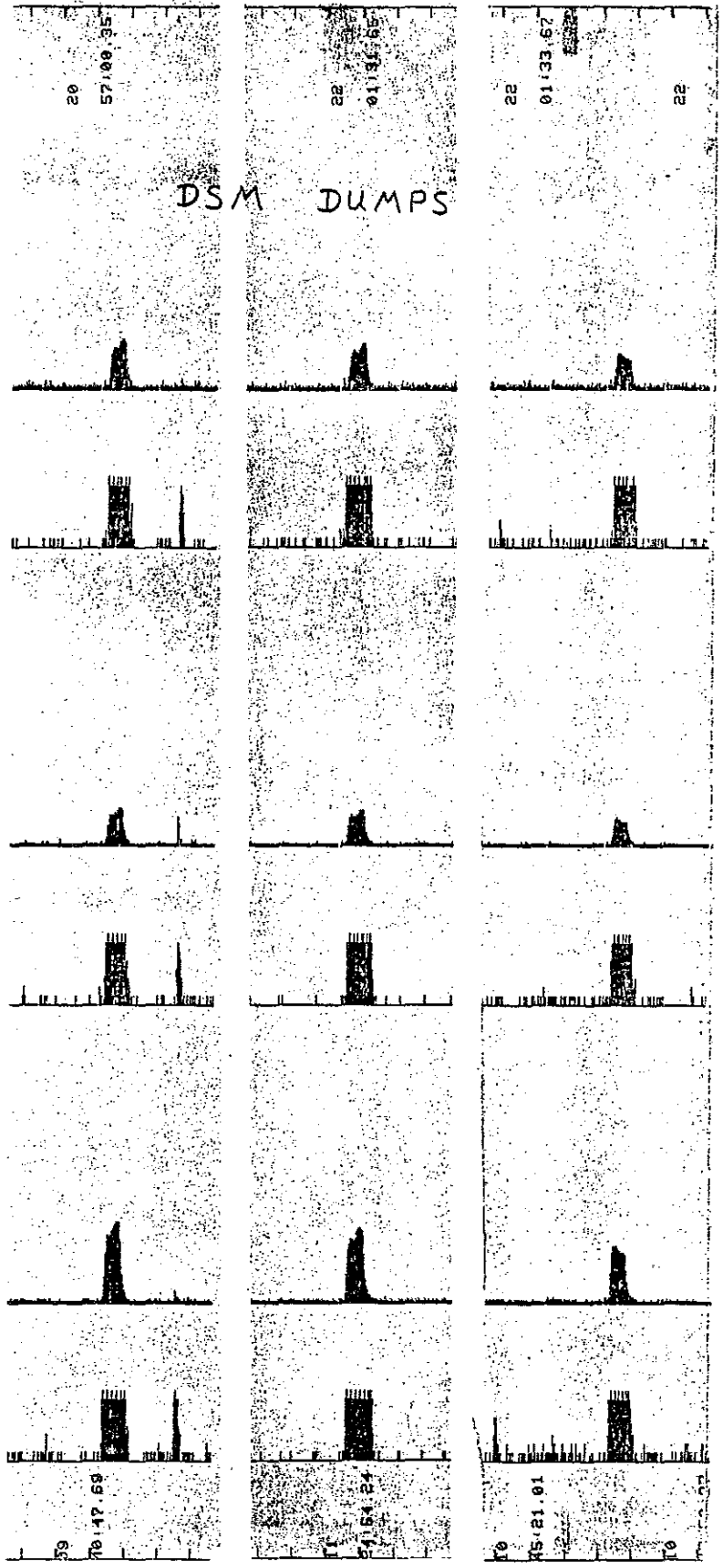


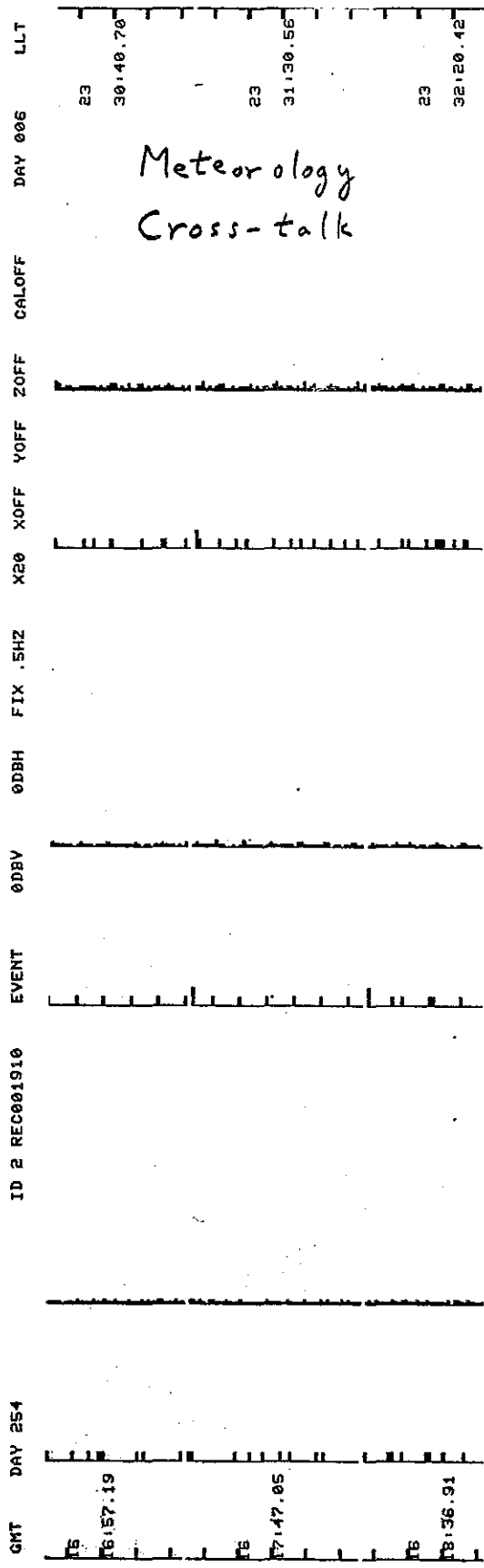


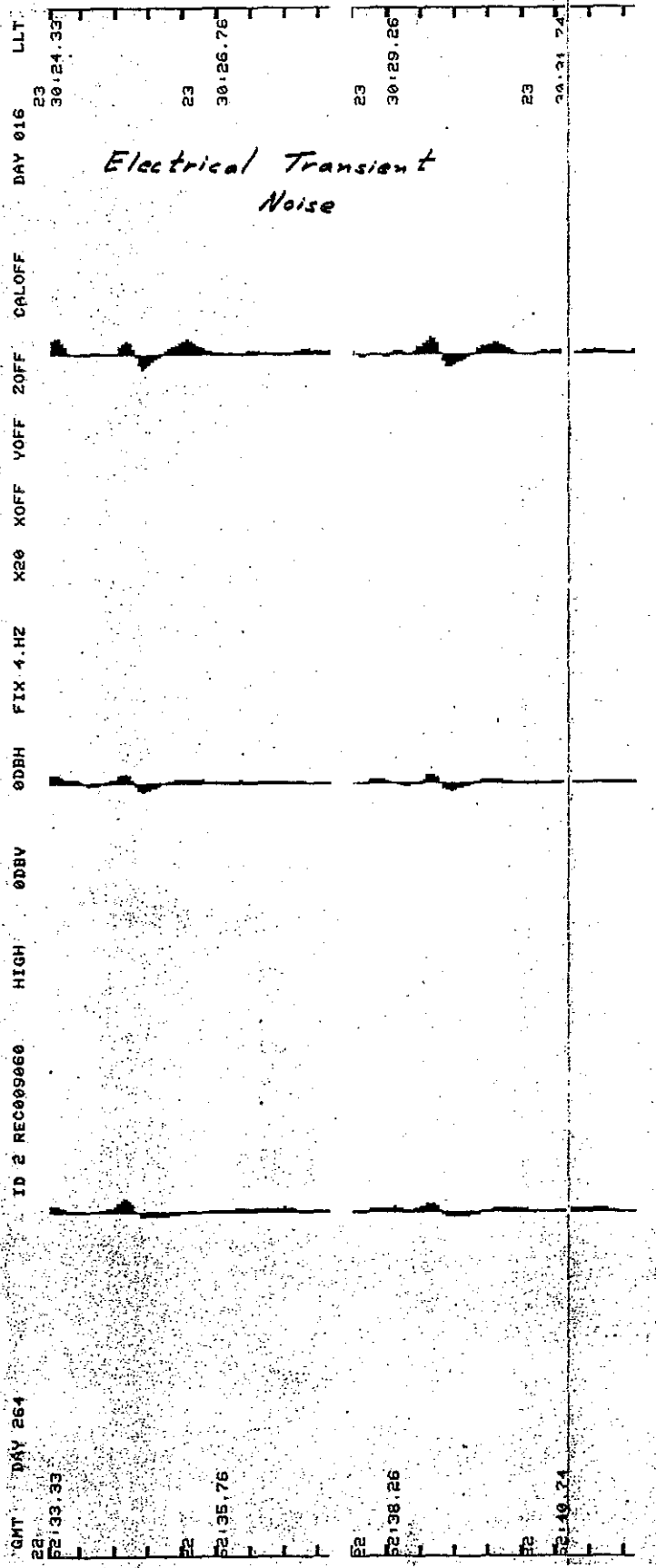
A-9

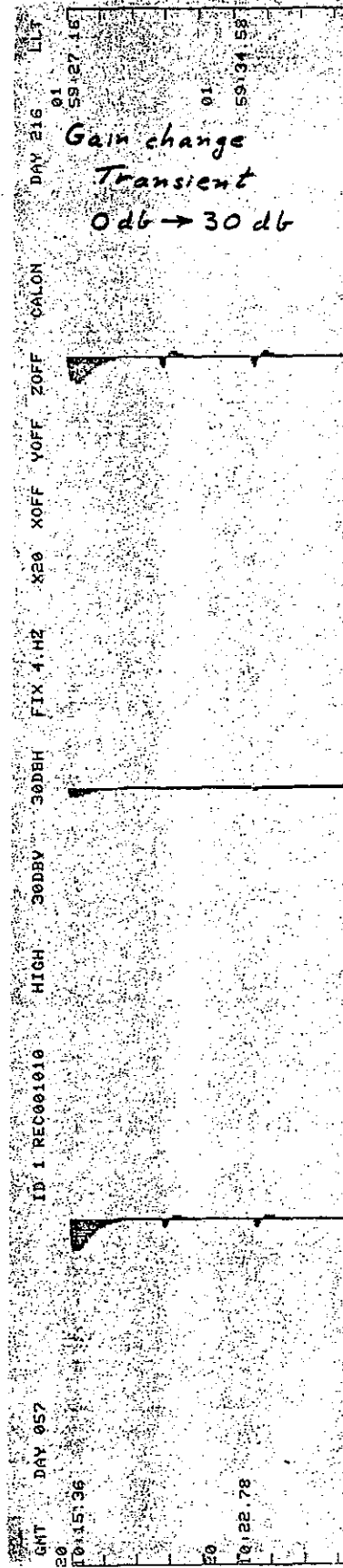
A-9

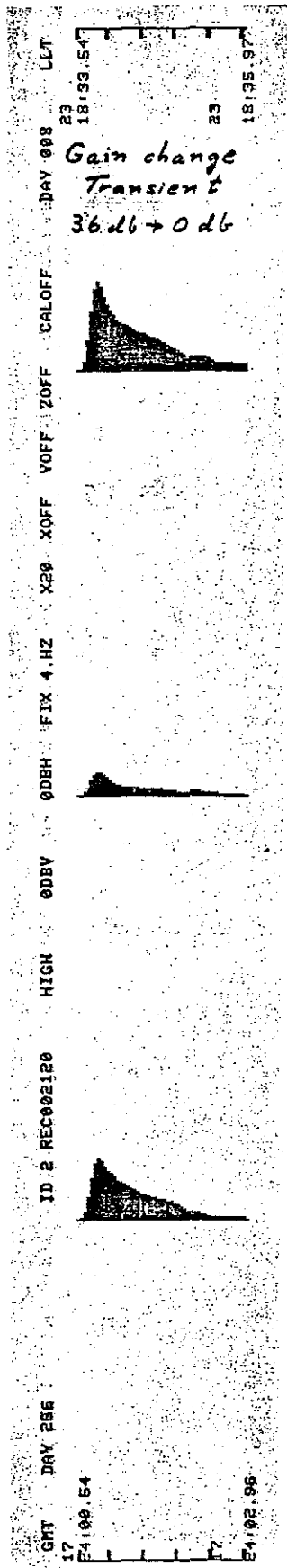
GNT DAY 360
 EVENT 0DBY
 0DBH STEP SHZ X20 XOFF YOFF ZOFF CALOFF DAY 109 LDT

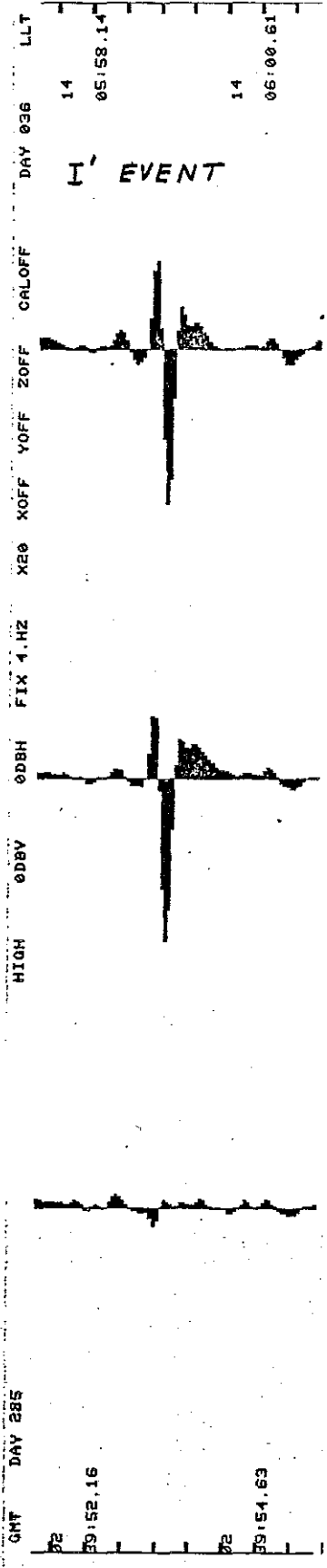




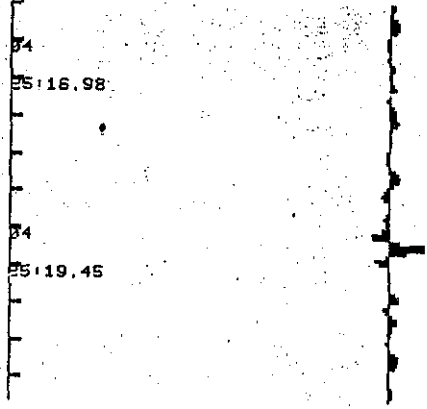




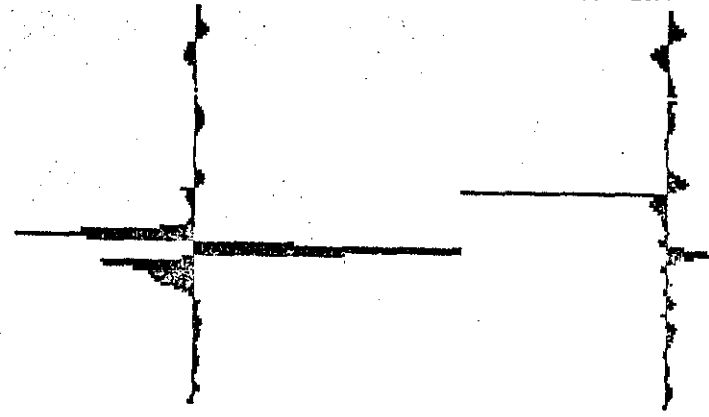




GMT DAY 287



HIGH 0DBV 0DBH FIX 4.HZ X20 XOFF YOFF ZOFF CALOFF



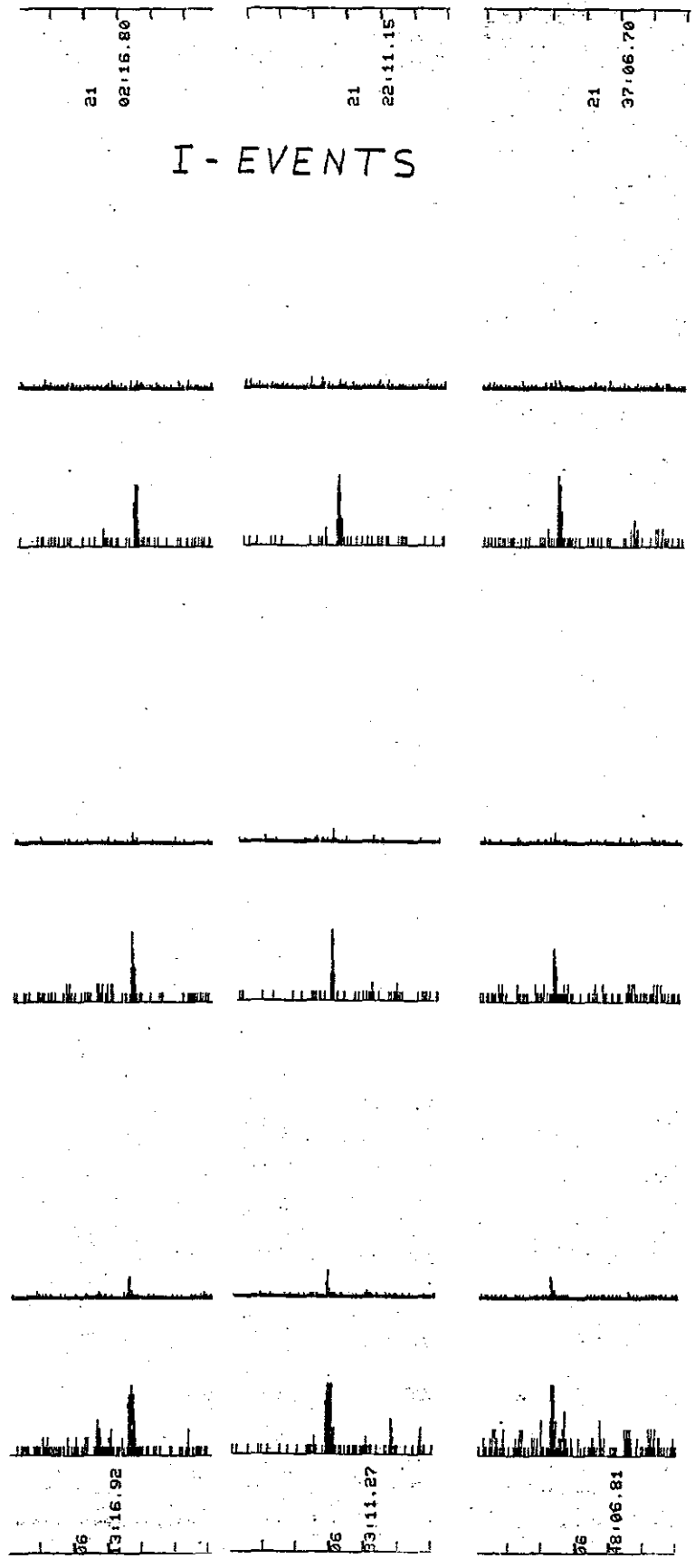
DAY 038 LLT

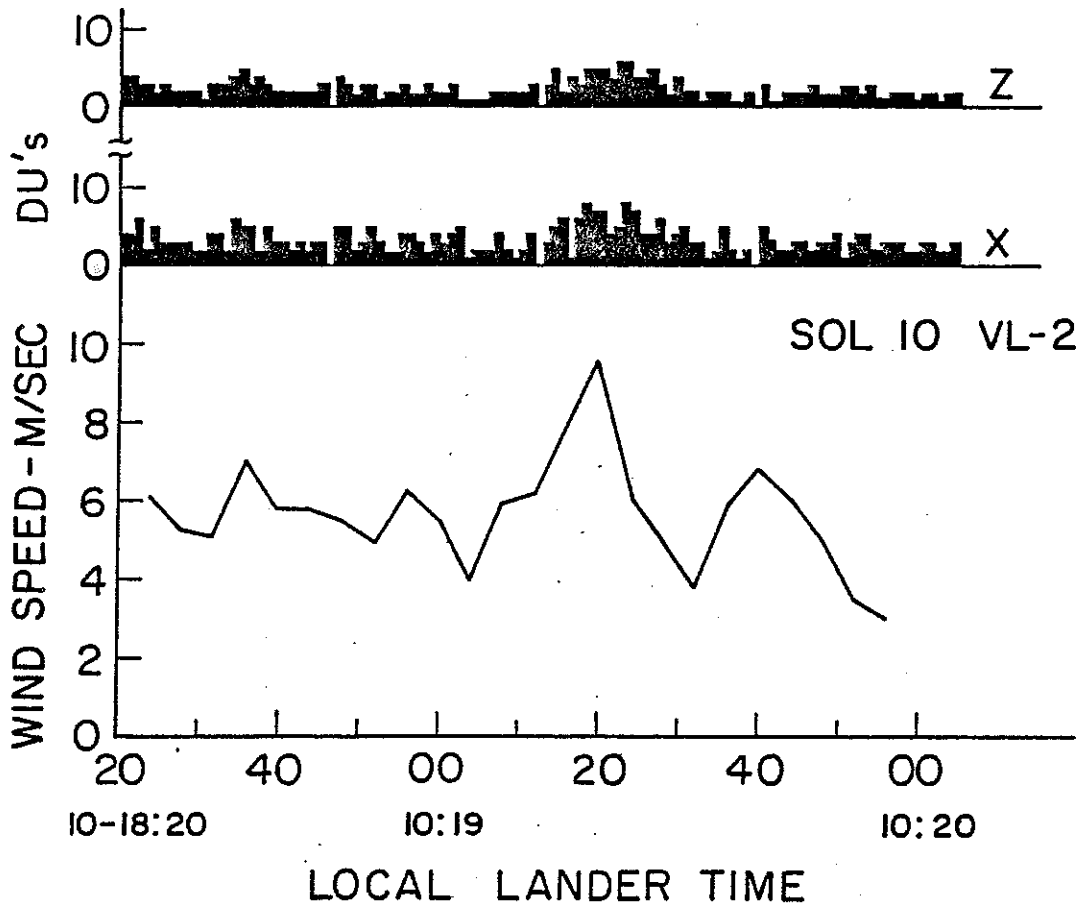
I' EVENT

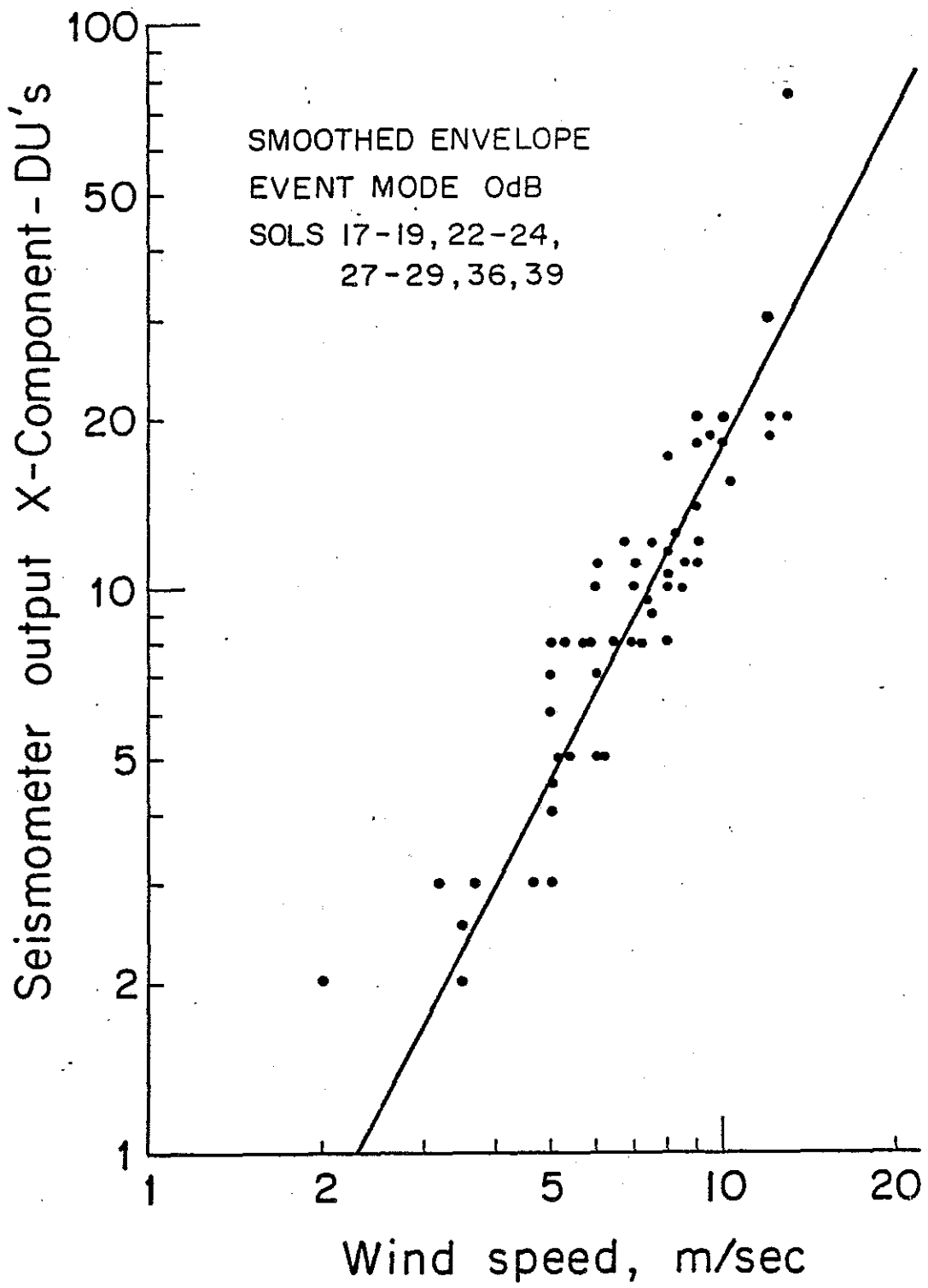
14
32:12.46
14
32:14.93

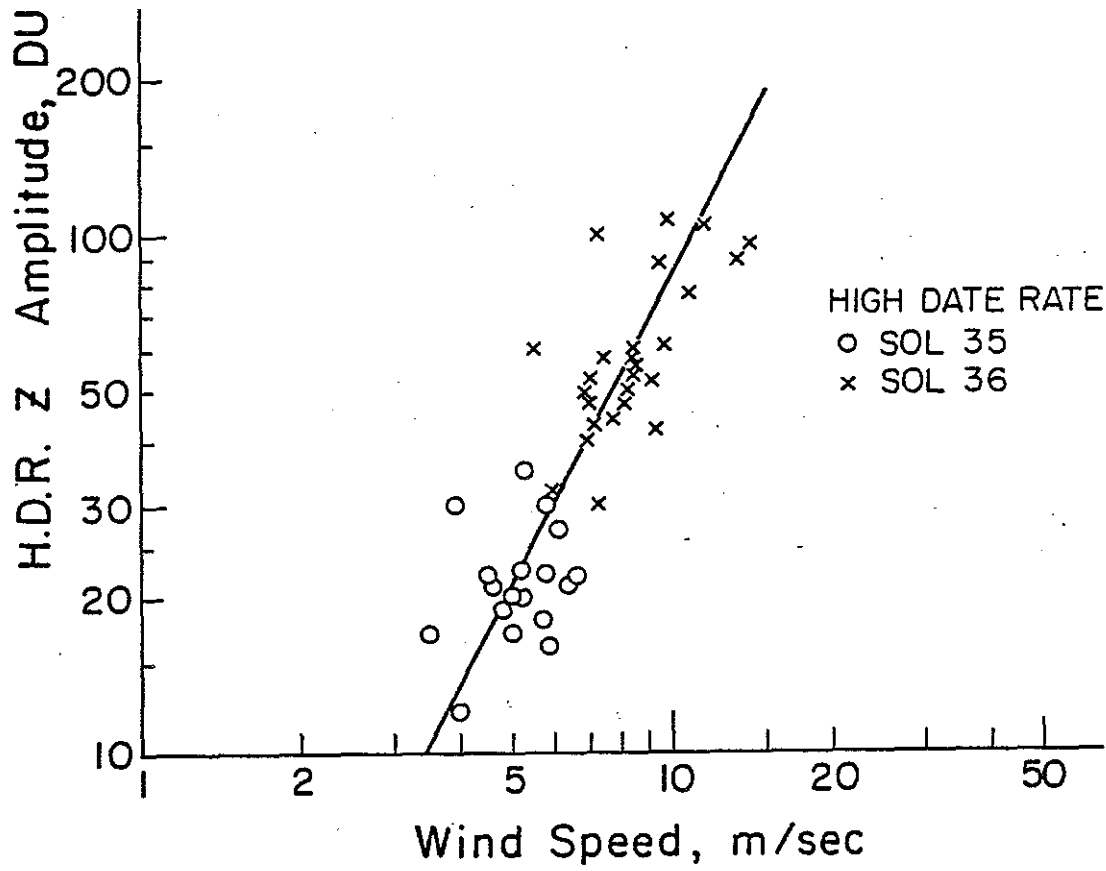
A-16

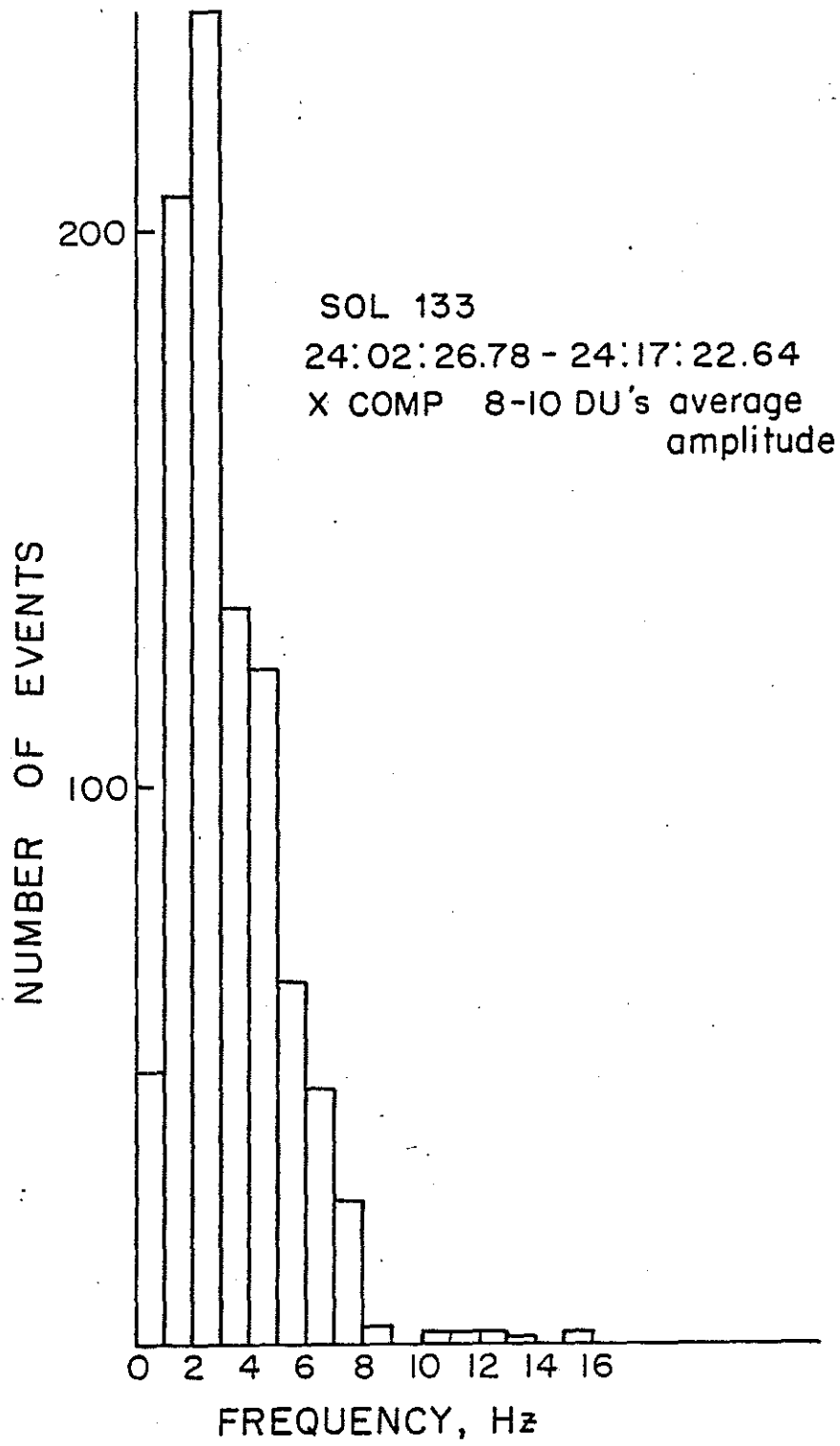
GMT DAY 026 DAY 140 LLT
EVENT 0DBV 0DBH FIX .5HZ X20 XOFF YOFF ZOFF CALOFF

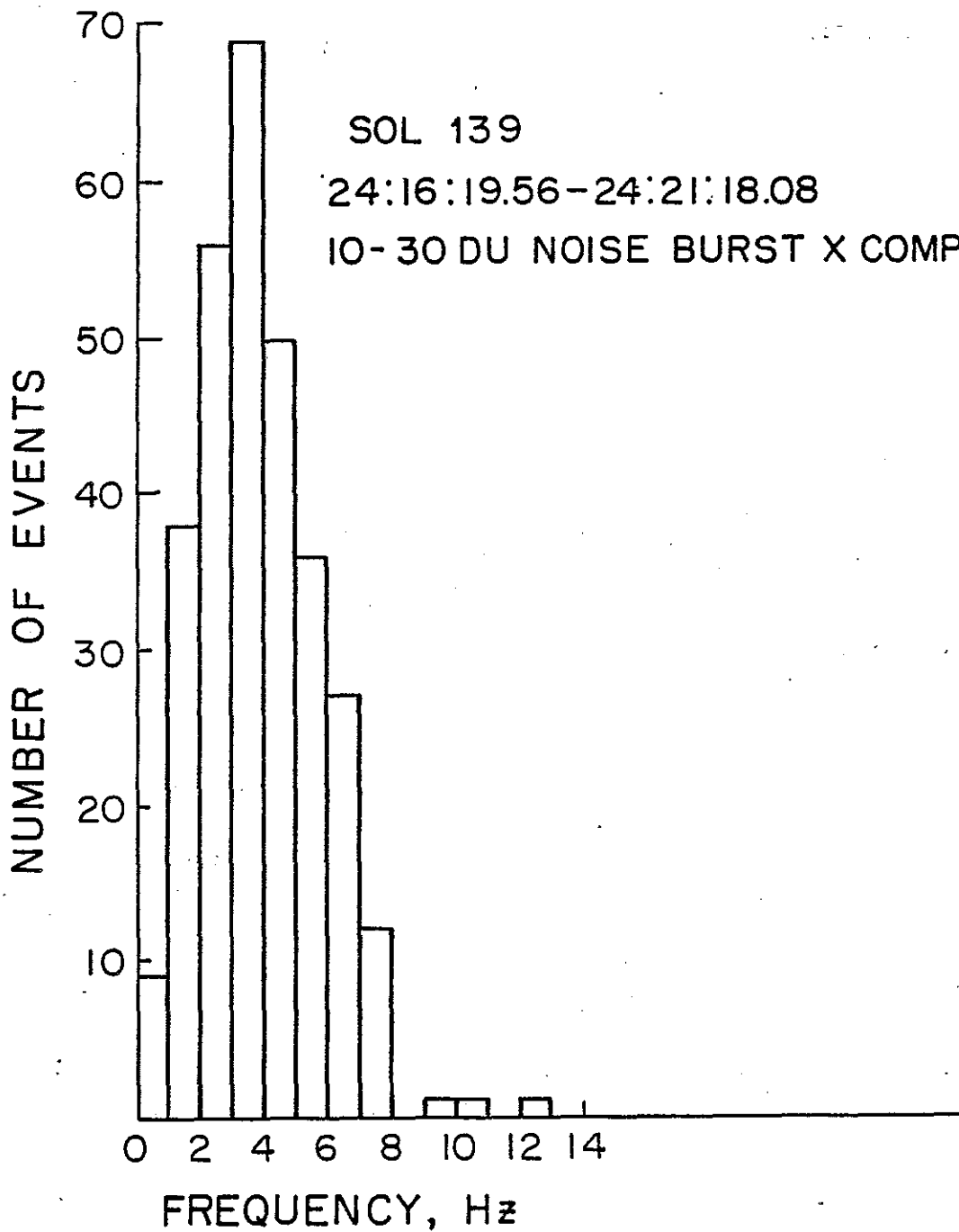




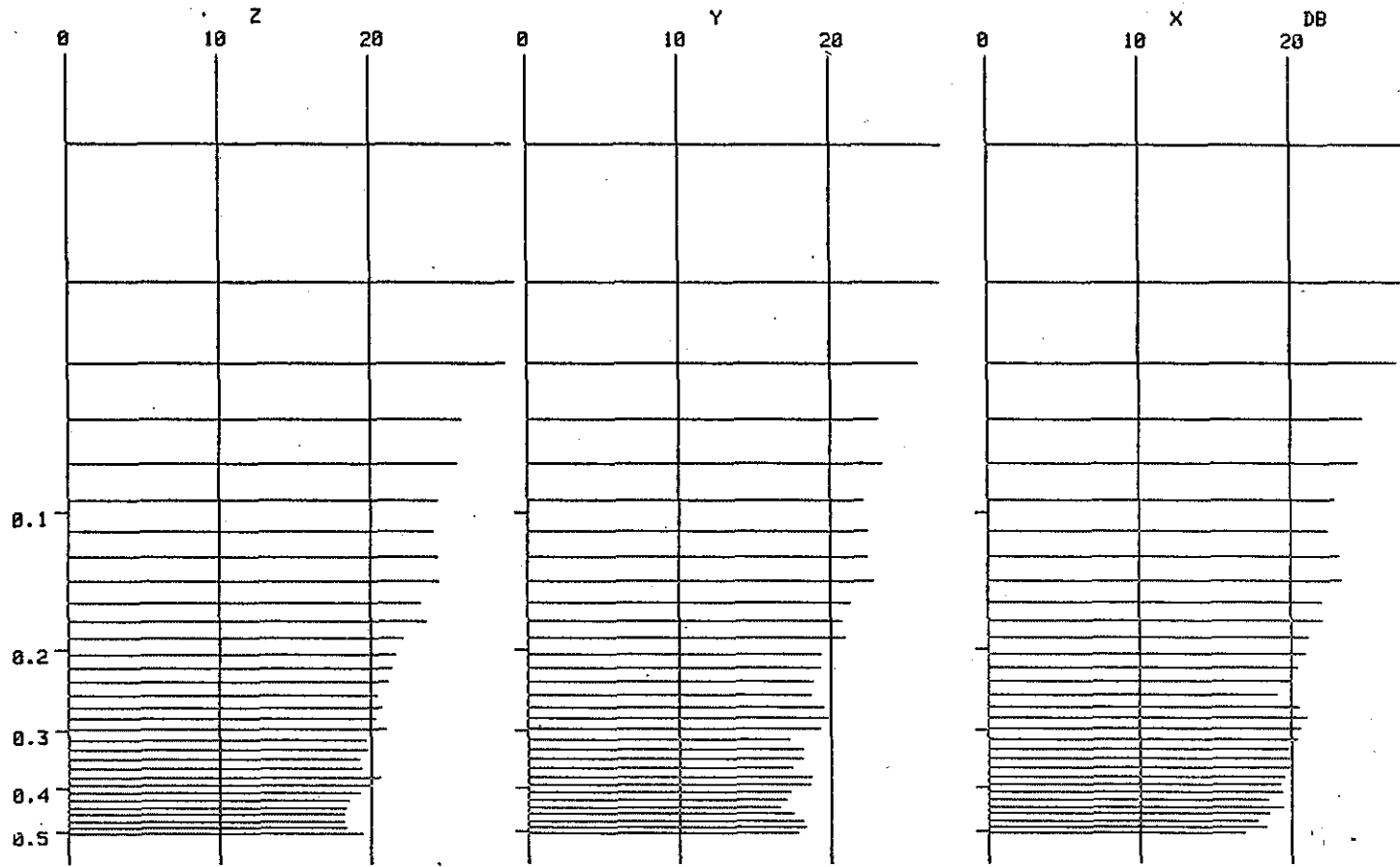








131 2109 2



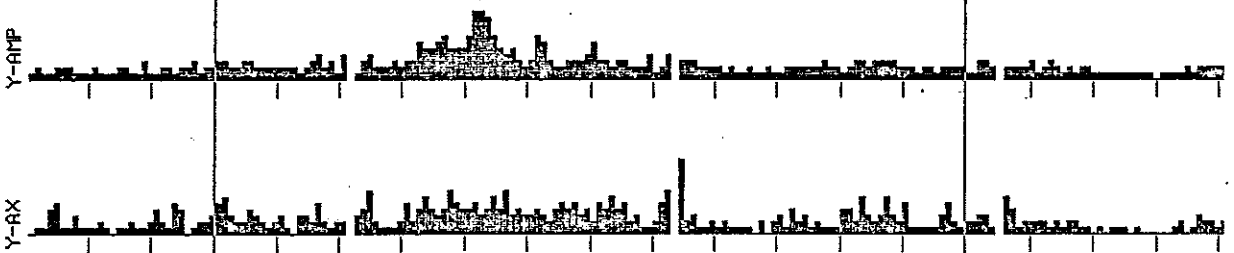
5560	5851	4903	2981	2760	1939	1766	2043	2153	1591	1605	1294	1244	1113	1002	798
1124	1264	1172	1080	934	975	960	901	844	853	698	875	715	593	690	498
5434	5249	3036	2076	2191	1648	1753	1753	1929	1363	1188	1239	857	856	760	732
907	960	864	537	660	659	561	752	736	541	507	466	575	650	685	611
8517	9004	7864	3987	3720	2790	2582	2786	2882	2171	2343	1653	1465	1380	1316	1122
1281	1073	1267	919	945	846	863	1150	1018	846	711	687	673	671	686	871

SOL 12
16:50

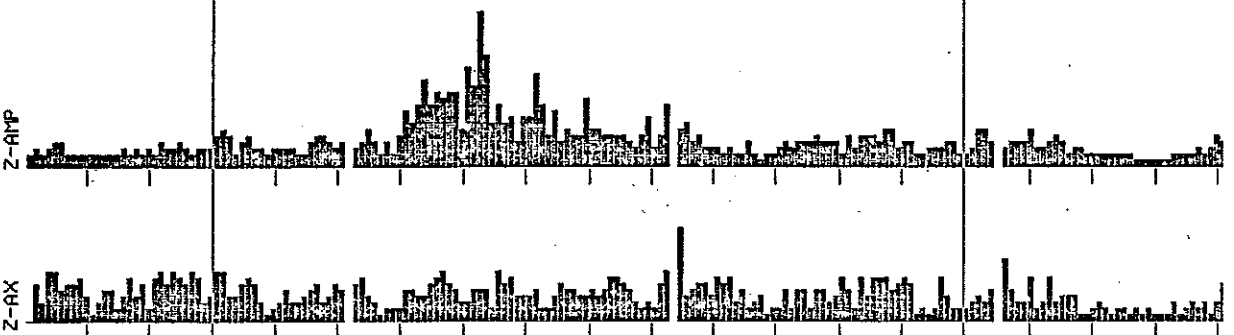
X



Y



Z

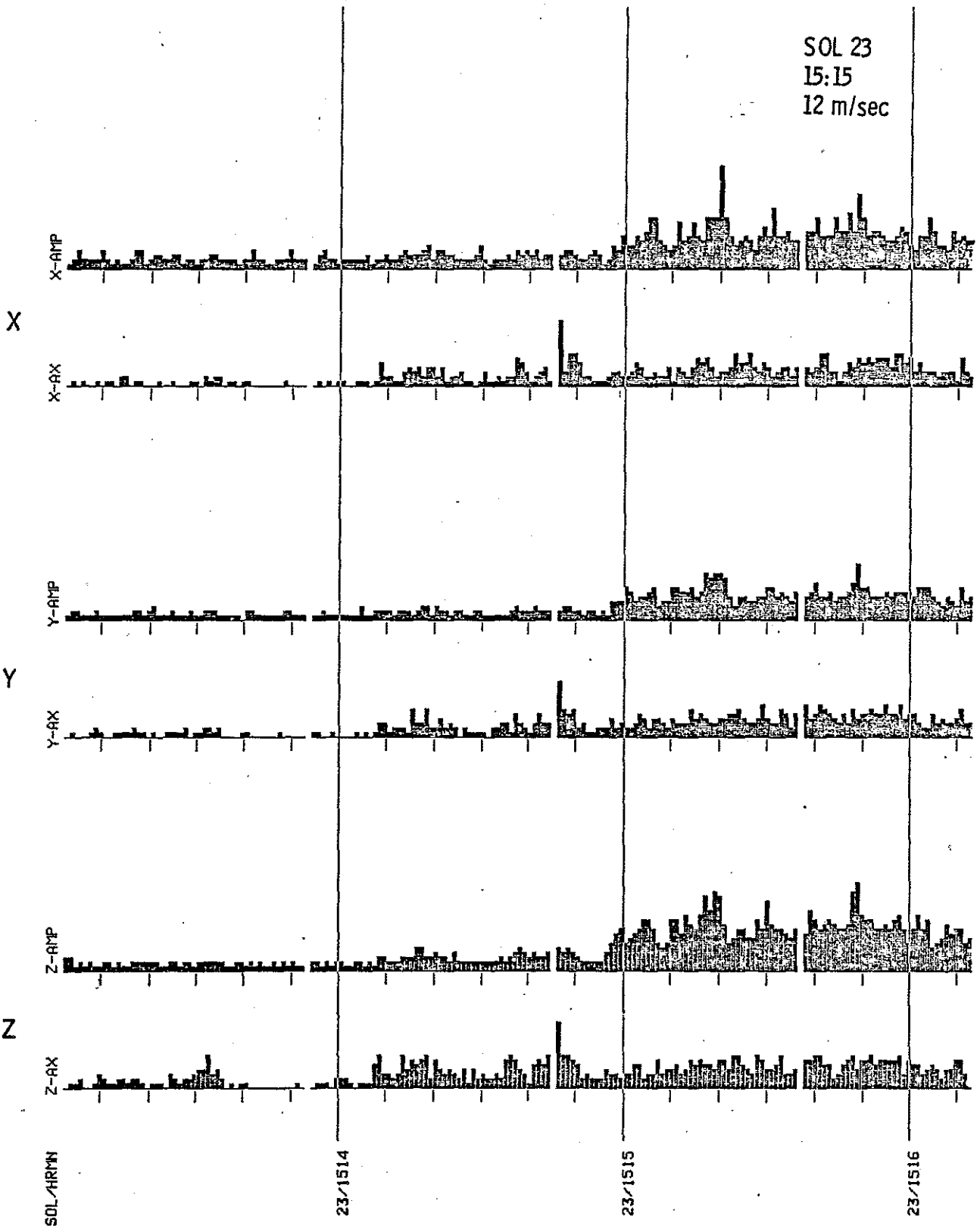


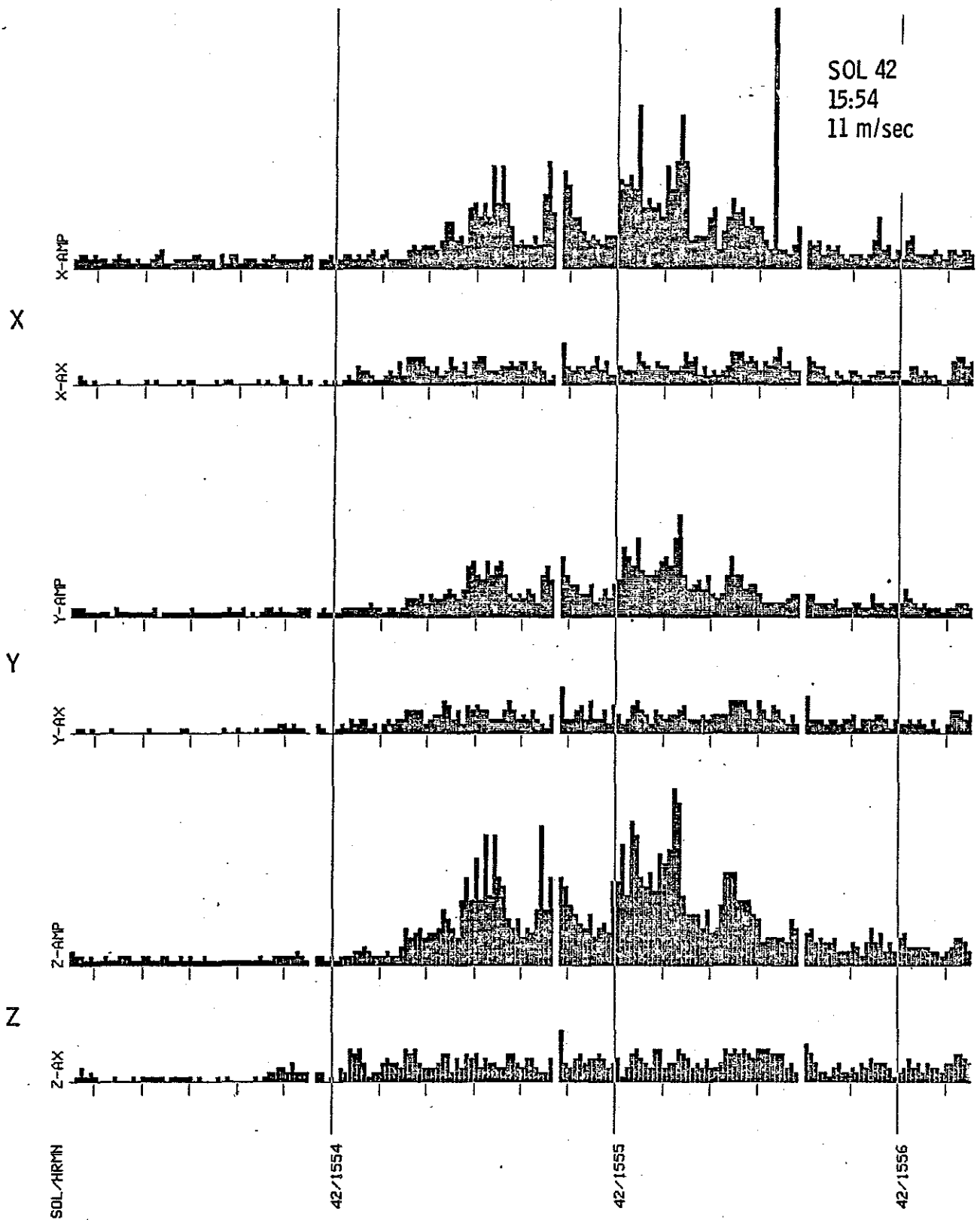
SOL/HR:MM

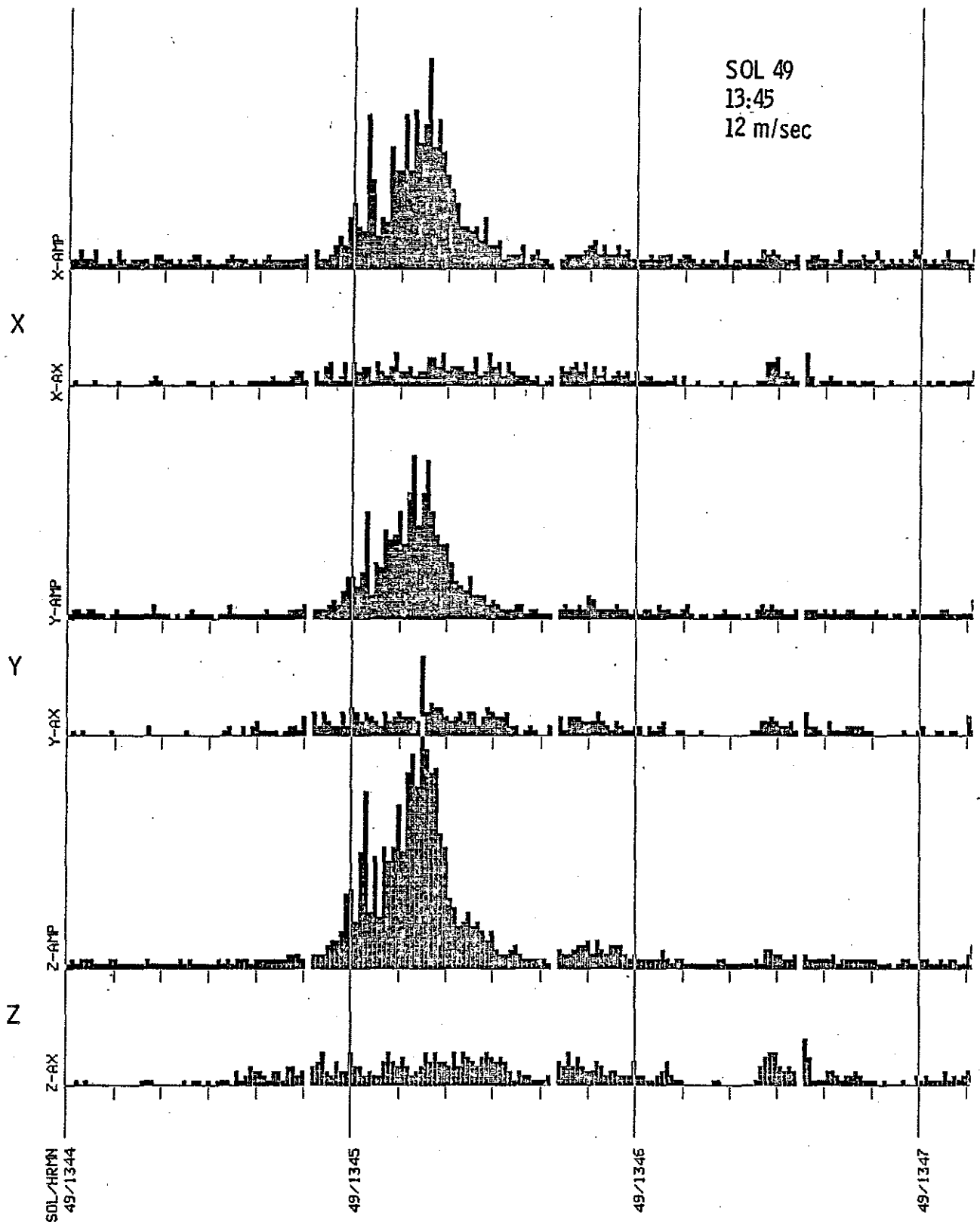
12/1650

12/1652

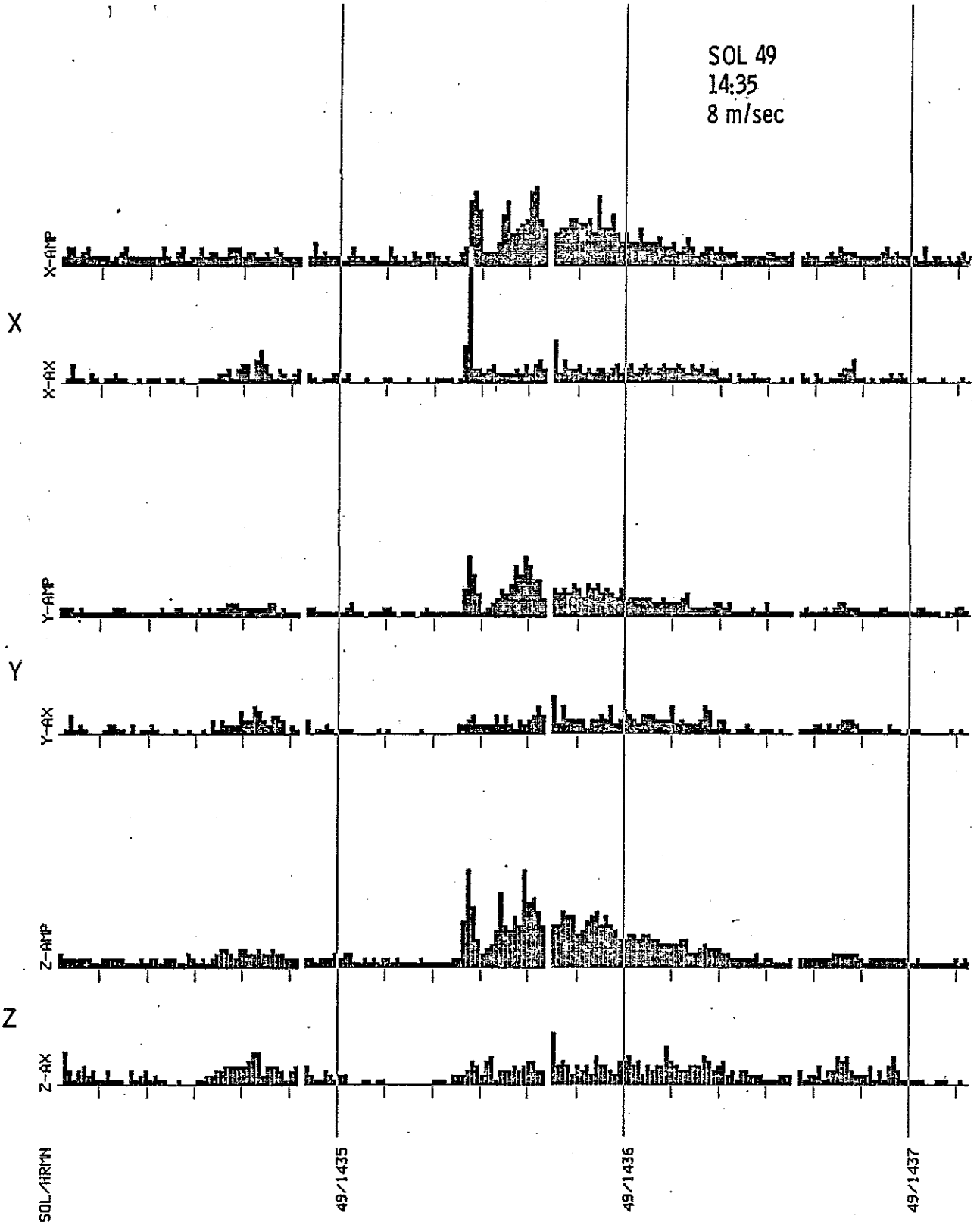
SOL 23
15:15
12 m/sec







SOL 49
14:35
8 m/sec



SOL 49
15:48
10 m/sec

